Research Article Vol. 32, No. 11 / 20 May 2024 / Optics Express 20136
Optics EXPRESS

Infrared phase-change chiral metasurfaces with tunable circular dichroism

HAOTIAN TANG,[1] LILIANA STAN,[2] DAVID A. CZAPLEWSKI,[2] XIAODONG YANG,[1,4] AND JIE GAO[3,5]

[1]Department of Mechanical and Aerospace Engineering, Missouri University of Science and Technology, Rolla, MissouriI 65409, USA
[2]Center for Nanoscale Materials, Argonne National Laboratory, Argonne, Illinois 60439, USA
[3]Department of Mechanical Engineering, Stony Brook University, Stony Brook, New York 11794, USA
[4]yangxia@mst.edu
[5]jie.gao.5@stonybrook.edu

Abstract: Integrating phase-change materials in metasurfaces has emerged as a powerful strategy to realize optical devices with tunable electromagnetic responses. Here, phase-change chiral metasurfaces based on GST-225 material with the designed trapezoid-shaped resonators are demonstrated to achieve tunable circular dichroism (CD) responses in the infrared regime. The asymmetric trapezoid-shaped resonators are designed to support two chiral plasmonic resonances with opposite CD responses for realizing switchable CD between negative and positive values using the GST phase change from amorphous to crystalline. The electromagnetic field distributions of the chiral plasmonic resonant modes are analyzed to understand the chiroptical responses of the metasurface. Furthermore, the variations in the absorption spectrum and CD value for the metasurface as a function of the baking time during the GST phase transition are analyzed to reveal the underlying thermal tuning process of the metasurface. The demonstrated phase-change metasurfaces with tunable CD responses hold significant promise in enabling many applications in the infrared regime such as chiral sensing, encrypted communication, and thermal imaging.

1. Introduction

Circular dichroism (CD) is a fundamental optical phenomenon arising when a material exhibits differential absorption of left- and right-handed circularly polarized (LCP and RCP) light [1]. CD spectroscopy has found widespread applications in various scientific disciplines including chemistry [2,3], biochemistry [4,5], and material science [6–8]. Recently, chiral optical metasurfaces have emerged as a promising platform to enhance CD spectroscopy in compact integrated photonic setups, based on their capabilities to manipulate circularly polarized light at the nanoscale and control the light polarization state efficiently [9–12]. Chiral metasurfaces consisting of subwavelength nanostructures with symmetry breaking patterns enable the precise chiroptical control of the amplitude, phase, and polarization of the incident light, which have been widely used in many fields such as chiral imaging [13,14], optical encryption [15,16], and optical communication [17]. Typically, phase-change materials can undergo structural phase transitions under external stimuli such as conductive heating or optical excitation [18,19]. In particular, GST-225 ($Ge_2Sb_2Te_5$) material has garnered considerable attention due to the high-contrast optical permittivity variation between the amorphous and the crystalline states, as well as its compatibility with photonic device integration [20,21]. The integration of phase-change materials in chiral metasurfaces will enable the active control and tuning of chiroptical properties of the metasurfaces. Such dynamic tunability allows on-demand manipulation and modulation of the circularly polarized light signal, which will empower advanced functionalities in a variety of applications such as high-resolution holograms [22], thermal imaging [23], biosensing [24], and

#525756 https://doi.org/10.1364/OE.525756
Journal © 2024 Received 4 Apr 2024; revised 6 May 2024; accepted 6 May 2024; published 15 May 2024

Optics EXPRESS

thermal camouflage [25]. However, chiral metasurfaces based on GST phase-change material with switchable CD values during a phase transition have not been widely studied yet.

Herein, we design and demonstrate infrared phase-change chiral metasurfaces based on GST-225 material with trapezoid-shaped resonators to realize tunable CD responses. The asymmetric trapezoid-shaped resonators are designed to support two chiral plasmonic resonances with opposite CD values under LCP and RCP illumination. Switchable CD between negative and positive values during the GST phase transition is realized by appropriately selecting the tilted angles of two slots in the metasurface unit cell design, where the peak wavelength of the plasmonic resonance under LCP excitation in the crystalline state overlaps with the peak wavelength under RCP excitation in the amorphous state. Furthermore, the electromagnetic field distributions of two chiral plasmonic resonant modes under LCP and RCP illumination are analyzed to elucidate the chiroptical responses of the metasurface. The absorption spectra and CD mapping of the metasurface at different baking times during the thermally induced phase transition of GST from amorphous to crystalline are analyzed to illustrate the thermal tuning process of chiral plasmonic resonance and CD value of the metasurface. The demonstrated results of infrared phase-change chiral metasurfaces enable the development of applications such as chiral molecular sensing, encrypted optical communication, thermal emitter, and thermal imaging.

2. Design and characterization of chiral metasurfaces with tunable CD

The schematic of the designed chiral metasurface is depicted in Fig. 1(a). The metasurface structure includes a 200 nm aluminum bottom mirror so that the transmitted light is eliminated and the absorption (A) of the metasurface structure can be obtained from the reflection (R) with A = 1 – R. Following this, a 75 nm GST-225 spacer layer is employed as the thermally induced phase transition material for achieving the metasurface tunability. A 15 nm alumina layer is then incorporated as a capping layer to prevent GST oxidation during the heating process [26]. Finally, a 60 nm aluminum top layer with trapezoid-shaped resonators is used to generate chiroptical responses of the metasurface. The metal-dielectric-metal structure forms a Fabry-Pérot cavity and enhances light absorption by multiple reflections of incident light [27]. The aluminum layers are deposited using electron beam evaporation. The GST-225 layer is deposited by RF sputtering of a GST-225 target using Ar. The alumina layer is grown by RF sputtering of an Al_2O_3 target. Only Ar gas is used for the first 3 nm to prevent oxidation of the GST-225, and then O_2 is introduced in the chamber to ensure the stoichiometry of the Al_2O_3. Figure 1(b) illustrates the dimensions of the metasurface unit cell with the periods of Px = 1.2 μm and Py = 0.4 μm. The designed trapezoid-shaped resonators with the height of A = 300 nm are formed by introducing two titled slots, which have the width of B = 104 nm and the tilted angles of $\alpha = 75°$ and $\beta = 45°$, respectively. The top base of the small trapezoid structure is C = 97 nm. The asymmetric arrangement of the slots with different tilted angles breaks the geometric symmetry, which leads to the chiroptical responses of the designed metasurface structures. The metasurface structures are milled in the top aluminum layer with a focused ion beam (FEI Helios Nanolab 600, 30 kV, 24 pA). The scanning electron microscope (SEM) image of the fabricated metasurface is displayed in Fig. 1(c).

GST-225 as a thermally induced phase transition material exhibits exceptional contrast of permittivity between amorphous and crystalline states. In the designed metasurface structure, the GST-225 layer serves as a dielectric spacer and enables the dynamic tuning capability of the chiral metasurface. The fabricated chiral metasurfaces are measured under LCP and RCP incident light to characterize their chiroptical responses. The absorption spectra of the metasurfaces are obtained with a Fourier-transform infrared spectroscopy system (FTIR, Nicolet 6700) connected to an infrared microscope. The circularly polarized light is defined by employing a combination of a broadband linear polarizer and a quarter-wave plate. The CD value in absorption is expressed

Optics EXPRESS

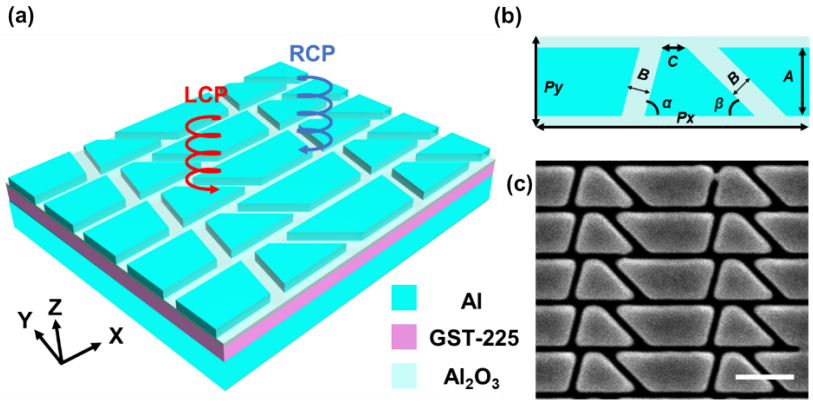

Fig. 1. (a) Schematic diagram of the GST-based phase-change chiral metasurface with tunable CD. (b) The dimensions of the metasurface unit cell. (c) SEM image of the chiral metasurface. Scale bar: 500 nm.

as CD = A_{LCP} - A_{RCP}. The measured absorption spectra of the metasurfaces with GST-225 in amorphous and crystalline states under LCP and RCP illumination are plotted in Fig. 2(a), while the corresponding CD spectra are shown in Fig. 2(b). With the GST-225 layer in the amorphous state at room temperature, there are two separated chiral plasmonic resonances with opposite CD responses supported in the metasurface structure, located at wavelengths of 2.564 μm and 2.838 μm under LCP and RCP excitation, respectively. The CD values are wavelength dependent and the peak CD values of approximately + 0.25 and − 0.35 are obtained at two chiral plasmonic resonances of 2.564 μm and 2.838 μm. By heating the metasurface at a temperature of 408 K for 16 minutes, the GST-225 layer experiences a phase transition from amorphous into crystalline. This increases the real part of the permittivity, which leads to the chiral plasmonic resonances redshifting to 2.838 μm and 3.082 μm under LCP and RCP illumination, respectively. Figure 2(b) shows that the CD spectrum is also redshifted to reach peak CD values of + 0.30 at 2.838 μm and − 0.32 at 3.082 μm. It is noted that the CD in absorption of the metasurface at the wavelength of 2.838 μm is switched from a negative value of − 0.35 to a positive value of + 0.30 with the GST phase change from amorphous to crystalline, as marked by the dashed line in Fig. 2(b). The simulated absorption spectra of the metasurface under LCP and RCP illumination using CST Studio Suite software are displayed in Fig. 2(c), and the simulated CD spectra are plotted in Fig. 2(d). In the simulation, the permittivity data of aluminum and alumina are obtained from previous work [28,29], while the permittivity of GST-225 is taken from Ref. [30]. It is shown that the simulated absorption spectra and CD spectra agree with the measured results, as the imaginary part of the aluminum permittivity is increased by a factor of two and the GST-225 permittivity under partial crystallization conditions is employed. The slight discrepancy between the simulated and measured spectra is related to defects and roughness of the metasurface structures introduced by the fabrication process.

To realize switchable CD between negative and positive values for the metasurfaces with GST phase transition at a specific wavelength, the asymmetric trapezoid-shaped resonators are designed to support two separated chiral plasmonic resonances with opposite CD responses, and the tilted angles of two slots α and β are selected appropriately. When α is equal to β, the symmetric trapezoid-shaped structure is formed, leading to the absorption of LCP light being equal to that of RCP light and thus no chiroptical response. By maintaining a constant β while varying the α value, the geometric symmetry of the trapezoid-shaped structure is broken so that the absorption values under LCP and RCP illumination are different which gives strong chiroptical response. Figure 3(a) and (c) depict the simulated peak wavelength positions of

Optics EXPRESS

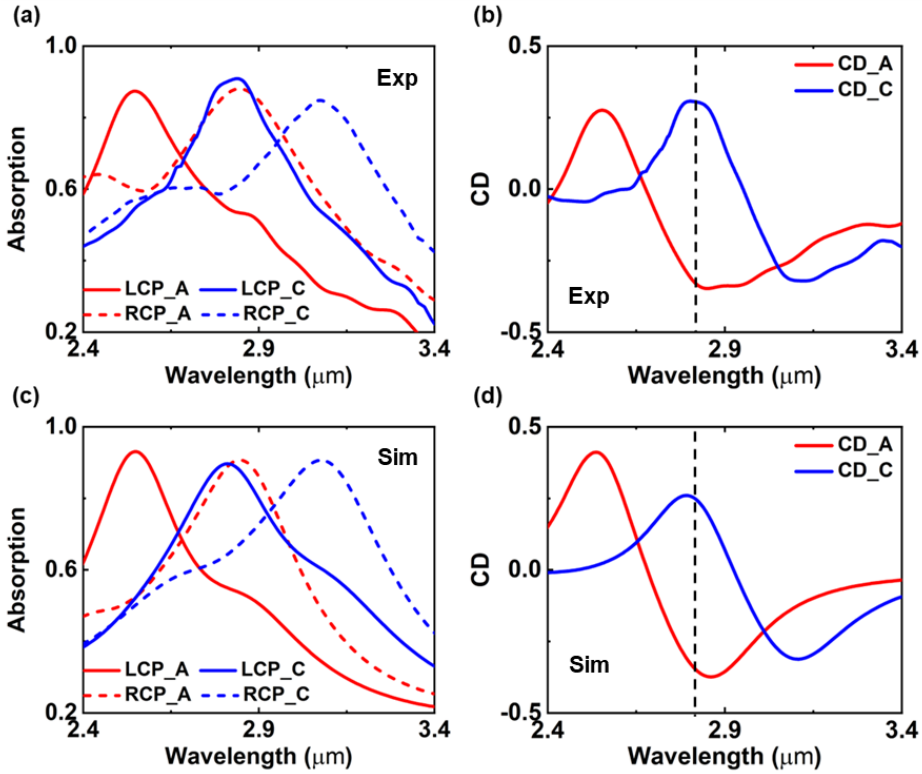

Fig. 2. Measured (a) absorption spectra under LCP and RCP illumination and (b) CD spectra of the metasurfaces with GST in amorphous and crystalline states. Simulated (c) absorption spectra and (d) CD spectra of the metasurfaces. The black dashed line marks the wavelength of 2.838 μm.

two chiral plasmonic resonances depending on the tilted angles of α and β for the metasurfaces with GST in amorphous and crystalline states. The α value varies from 35° to 80°, while the β value is kept as a constant of 35°, 45°, or 55°. For both amorphous and crystalline states, there is a gradual peak wavelength redshift for the plasmonic resonance under LCP excitation as α is reduced from 80° to 35° at a fixed β value, however, the peak wavelength of the plasmonic resonance under RCP excitation remains almost the same. On the other hand, the decrease of β value will induce a large peak wavelength redshift for the plasmonic resonance under RCP excitation, but only slightly affect the plasmonic resonance under LCP excitation. After the GST changes from amorphous to crystalline, both the chiral plasmonic resonances are redshifted due to the increased permittivity of the GST layer as shown in Fig. 3(c). Considering the above wavelength shift features of two chiral plasmonic resonances, switchable CD can be achieved by selecting the appropriate tilted angles of α and β so that the peak wavelength of the plasmonic resonance under LCP excitation in the crystalline state overlaps with that under RCP excitation in the amorphous state. As marked with a red diamond symbol in Fig. 3(a) and (c), when the α value is 75° and the β value is 45°, the peak wavelength of the plasmonic resonance under LCP in the crystalline state is almost equal to that under RCP in the amorphous state, which is at the wavelength of 2.838 μm. Figure 3(b) and (d) further present the CD spectrum mapping of the metasurfaces in both the amorphous and the crystalline states, with a fixed β value of 45° and the reduced α value from 80° to 35°. The CD spectrum mapping displays almost the maximum negative CD value of – 0.4 for the metasurface in the amorphous state close to the wavelength of

Optics EXPRESS

2.838 μm for the α value around 75°, while it exhibits a positive CD value around + 0.3 for the metasurface in the crystalline state, revealing a large CD value tuning from negative to positive with GST phase transition from amorphous to crystalline.

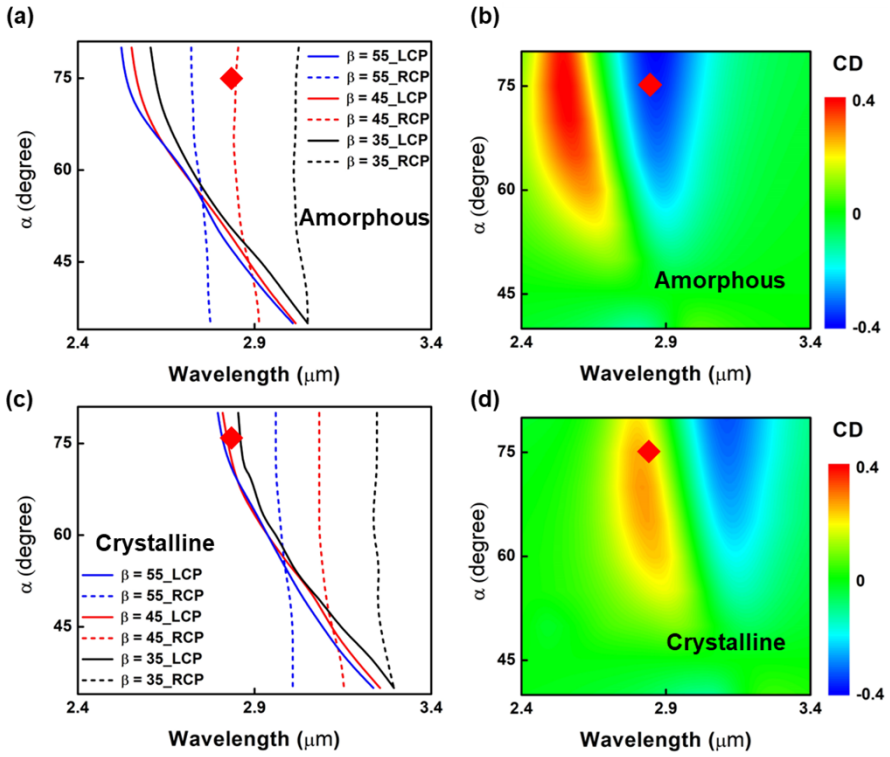

Fig. 3. Simulated peak wavelength positions of two chiral plasmonic resonances for the metasurfaces with GST in (a) amorphous state and (c) crystalline state with the α value varying from 35° to 80° while keeping the β value constant at 35°, 45°, or 55°. Simulated CD spectrum mapping of the metasurfaces in (b) amorphous state and (d) crystalline state with the fixed β value of 45° and the α value varying from 35° to 80°.

The two chiral plasmonic resonant modes with opposite CD responses under LCP and RCP illumination for the metasurface with the GST layer in the amorphous state are simulated with the COMSOL software, in order to further analyze the mechanism behind the chiroptical responses of the metasurface. Figure 4(a) displays the normalized electric field |E| distributions of the plasmonic resonant mode at the resonance wavelength of 2.564 μm at the interface between the GST layer and the alumina layer in the X-Y plane. The LCP incident light strongly excites the plasmon resonance mode with the field concentration mainly around the large trapezoid structure. However, the RCP incident light couples majorly to the small trapezoid structure with a weak coupling strength. As a result, a higher absorption of LCP light is achieved compared to RCP light which gives a positive CD response. Figure 4(b) further presents the normalized electric field distributions in the cross-sectional X-Z plane. The electric field under LCP illumination is concentrated around the large trapezoid structure within the alumina layer, whereas the much weaker electric field is located around the small trapezoid structure under RCP illumination. Figure 4(c) shows the magnetic field |H| and displacement current distributions in the cross-sectional X-Z plane. Compared to the RCP light, the LCP incident light strongly excites the magnetic dipole modes inside the GST layer. Three circulating current loops are formed around the magnetic dipole modes, with two strong current loops underneath the large trapezoid

Optics EXPRESS

structure, which contributes to the high absorption of LCP incident light. Figure 4(d)-(f) shows the corresponding field distributions of the plasmonic resonant mode at the resonance wavelength of 2.838 μm. The coupling of the RCP light to the plasmonic resonant mode is much stronger than that of the LCP light, with the highly concentrated electric field located around the small trapezoid structure in the alumina layer, as displayed in Fig. 4(d) and (e). Hence, the absorption of RCP light is higher than that of LCP light which leads to a negative CD response. As shown in Fig. 4(f), the magnetic dipole modes inside the GST layer are strongly excited by the RCP light rather than the LCP light, with two circulating current loops formed and one strong current loop below the small trapezoid structure, which leads to the high absorption of RCP light. It is noted that the field distributions of two chiral plasmonic resonant modes under LCP and RCP illumination for the metasurface with the GST layer in the crystalline state will be very similar to those in the amorphous state, but with the plasmonic resonance wavelengths redshifted to 2.838 μm and 3.082 μm, respectively.

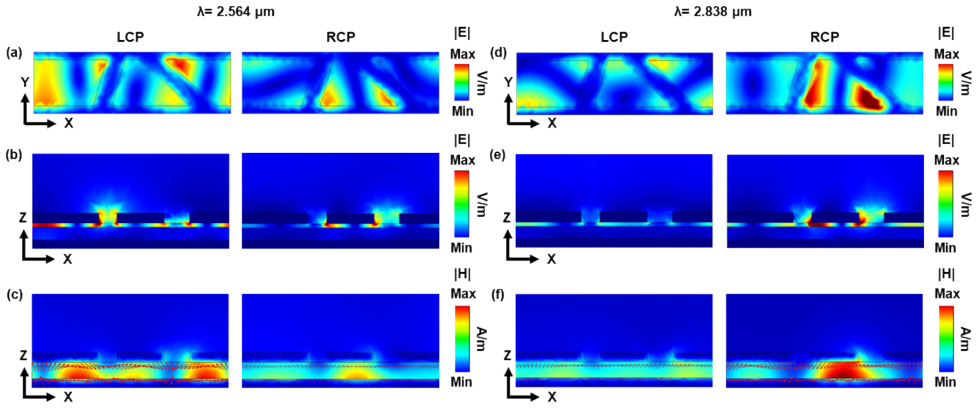

Fig. 4. (a),(d) Simulated electric field |E| distributions of two plasmonic resonant modes at the resonance wavelengths of 2.564 μm and 2.838 μm at the interface between GST layer and alumina layer under LCP and RCP incident light. (b),(e) Simulated electric field |E| distributions of two plasmonic resonant modes along the cross-sectional plane. (c),(f) Simulated magnetic field |H| and displacement current distributions of two plasmonic resonant modes along the cross-sectional plane. The red arrows represent the magnitude and direction of displacement current.

In order to study the thermal tunning process of the chiral metasurface induced by the phase transition of the GST layer from amorphous to crystalline, the absorption spectra of the chiral metasurface are characterized when the metasurface is subjected to heating at a temperature of 408 K, which is above the GST phase transition temperature [31]. The absorption spectra are recorded after baking the metasurface for two minutes and then cooling down to room temperature. Such measurements are repeated until there is no future wavelength shift in the absorption spectrum. A series of measured and simulated absorption spectra of the chiral metasurface at different baking times from 0 to 16 minutes are depicted in Fig. 5(a) and (b), revealing the thermal tuning effects of two chiral plasmonic resonances across the wavelength range of 2.4 μm to 3.4 μm. For the metasurface with the GST layer in the amorphous state, the plasmonic resonance under LCP excitation is located at 2.564 μm, while the plasmonic resonance under RCP excitation is positioned at 2.838 μm. It is observed that both the chiral plasmonic resonances exhibit wavelength redshifts as the baking time increases, which shows dynamic thermal tuning of the chiral metasurface due to the increased permittivity of the GST layer during the phase change from amorphous to crystalline. The plasmonic resonance under LCP excitation is redshifted progressively from 2.564 μm before baking to around 2.838 μm after a baking time

Optics EXPRESS

of 16 minutes, which almost overlaps with the plasmonic resonance under RCP excitation present in the amorphous state before baking. Meanwhile, the plasmonic resonance under RCP excitation experiences a gradual redshift from 2.838 μm to 3.082 μm as the baking time increases from 0 to 16 minutes. It is found that the absorption levels of both chiral plasmonic resonances are maintained during the thermal tuning process of the metasurface.

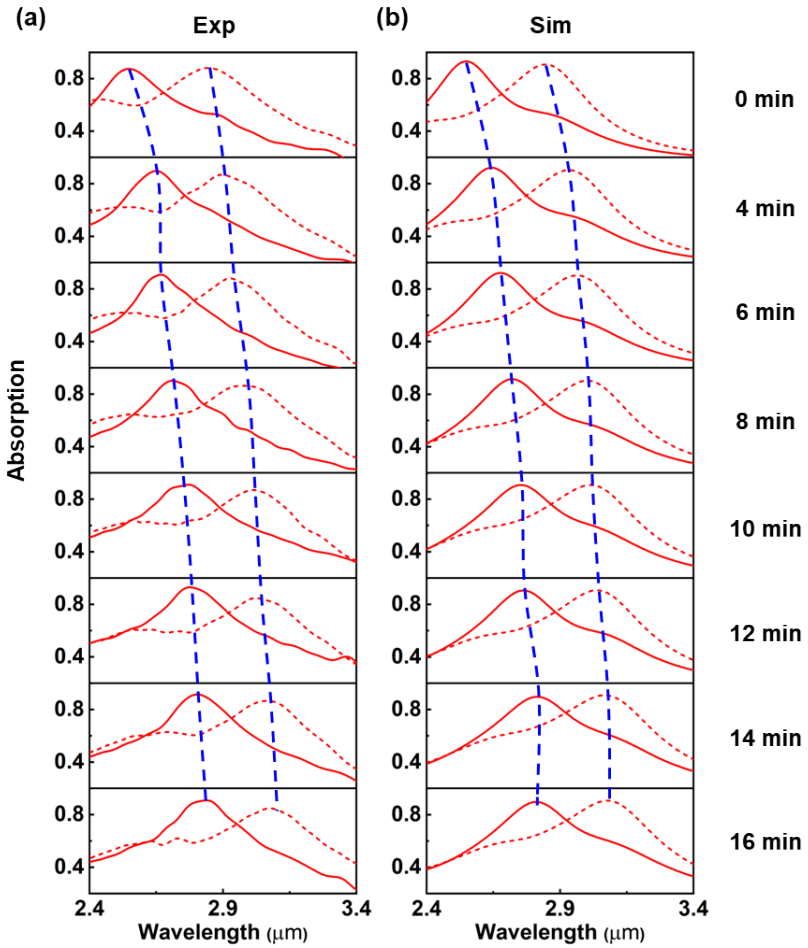

Fig. 5. (a) Measured absorption spectra of the chiral metasurface at different baking times from 0 to 16 minutes at the temperature of 408 K. (b) Simulated absorption spectra of the metasurface at different baking times. The red solid (dashed) lines indicate the absorption spectra under LCP (RCP) illumination. The blue dashed lines mark the peak wavelength positions of two chiral plasmonic resonances.

The wavelength redshifts of the chiral plasmonic resonances resulting from the thermally induced GST phase transition further leads to significant changes in the CD responses of the chiral metasurface. Figure 6(a) and (b) plot the measured and simulated CD mapping of the metasurface at varying baking times, showing the evolution of the CD values depending on both the wavelength and the baking time. Specifically, the metasurface with GST in the amorphous state before baking exhibits zero CD value at a wavelength of 2.68 μm and a negative CD response above that wavelength. As the baking time increases, the CD spectrum of the metasurface redshifts and the wavelength position for zero CD value is also gradually increased. The metasurface with GST in

Optics EXPRESS

the crystalline state at the baking time of 16 minutes has zero CD value around a wavelength of 2.95 μm and a positive CD response below that wavelength. Therefore, a switchable CD response from negative to positive is observed within the wavelength range of 2.68 μm to 2.95 μm as the GST phase transition occurs from amorphous to crystalline, where the maximum change in CD value is achieved at the wavelength of 2.838 μm. Figure 6(c) displays the measured and simulated CD values at the wavelength of 2.838 μm under various baking times, showing the continuous increase of CD from a negative value of − 0.35 to a positive value of + 0.30 during the GST phase change. It shows that there is a good agreement between the experimental data and the simulated results.

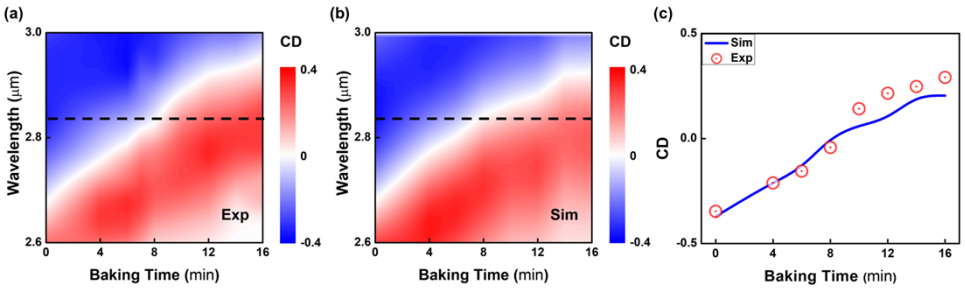

Fig. 6. (a) Measured and (b) simulated CD mapping of the metasurface at varying baking times at 408 K. The black dashed line marks the wavelength of 2.838 μm where the maximum change in CD value is achieved. (c) CD values of the metasurface at the wavelength of 2.838 μm at different baking times.

3. Conclusion

In summary, infrared phase-change chiral metasurfaces with trapezoid-shaped resonators have been demonstrated to achieve tunable CD responses. The asymmetric trapezoid-shaped resonators are designed to support two chiral plasmonic resonances with opposite CD responses. Switchable CD between negative and positive values for the metasurface at a specific wavelength is realized by selecting the appropriate tilted angles of two slots so that the peak wavelength of the plasmonic resonance under LCP excitation in the crystalline state overlaps with that under RCP excitation in the amorphous state. The electromagnetic field distributions of two chiral plasmonic resonant modes under LCP and RCP illumination are analyzed to understand the chiroptical responses of the metasurface. Moreover, the evolution of absorption spectra and CD values for the metasurface during the GST phase transition from amorphous to crystalline are studied to reveal the thermal tuning process of chiral plasmonic resonance and CD value as a function of the baking time. It is noteworthy that the photothermally induced phase change in GST is reversible and the switching speed can happen in the order of picoseconds to nanoseconds, which depends on the thermal conductance of materials, the laser pulse duration, and the laser intensity [32,33]. This feature of GST phase change will enable the realization of dynamically modulated and switchable chiral metasurfaces in the future. The demonstration of the phase-change chiral metasurfaces with switchable CD responses presents the potential for advancing various applications such as chiral sensing, encrypted communication, thermal emitter, thermal imaging, and temperature sensing.

Funding. National Science Foundation (ECCS-2230069, ECCS-2230071); U.S. Department of Energy (DE-AC02-06CH11357).

Acknowledgments. Work performed at the Center for Nanoscale Materials, a U.S. Department of Energy Office of Science User Facility, was supported by the U.S. DOE, Office of Basic Energy Sciences, under Contract No. DE-AC02-06CH11357. The authors acknowledge the support from the Intelligent Systems Center and the facility support from the Materials Research Center at Missouri S&T.

Optics EXPRESS

Disclosures. The authors declare no conflicts of interest.

Data availability. Data underlying the results presented in this paper are not publicly available at this time but may be obtained from the authors upon reasonable request.

Reference

1. S. Hashiyada, T. Narushima, and H. Okamoto, "Imaging chirality of optical fields near achiral metal nanostructures excited with linearly polarized light," ACS Photonics **5**(4), 1486–1492 (2018).
2. A. J. Miles and B. A. Wallace, "Circular dichroism spectroscopy of membrane proteins," Chem. Soc. Rev. **45**(18), 4859–4872 (2016).
3. C. Merten, T. P. Golub, and N. M. Kreienborg, "Absolute configurations of synthetic molecular scaffolds from vibrational CD spectroscopy," J. Org. Chem. **84**(14), 8797–8814 (2019).
4. E. Aronoff-Spencer, C. S. Burns, N. I. Avdievich, *et al.*, "Identification of the Cu2 + binding sites in the N-terminal domain of the prion protein by EPR and CD spectroscopy," Biochem. **39**(45), 13760–13771 (2000).
5. Z. Cao, H. Gao, M. Qiu, *et al.*, "Chirality Transfer from Sub-Nanometer Biochemical Molecules to Sub-Micrometer Plasmonic Metastructures: Physiochemical Mechanisms, Biosensing, and Bioimaging Opportunities," Adv. Mater. **32**(41), 1907151 (2020).
6. J. Hu, M. Lawrence, and J. A. Dionne, "High quality factor dielectric metasurfaces for ultraviolet circular dichroism spectroscopy," ACS Photonics **7**(1), 36–42 (2020).
7. W. J. Choi, G. Cheng, Z. Huang, *et al.*, "Terahertz circular dichroism spectroscopy of biomaterials enabled by kirigami polarization modulators," Nat. Mater. **18**(8), 820–826 (2019).
8. J. Lasa-Alonso, D. R. Abujetas, Á. Nodar, *et al.*, "Surface-enhanced circular dichroism spectroscopy on periodic dual nanostructures," ACS Photonics **7**(11), 2978–2986 (2020).
9. X. Zhang, Y. Liu, J. Han, *et al.*, "Chiral emission from resonant metasurfaces," Sci **377**(6611), 1215–1218 (2022).
10. K. Tanaka, D. Arslan, S. Fasold, *et al.*, "Chiral bilayer all-dielectric metasurfaces," ACS Nano **14**(11), 15926–15935 (2020).
11. C. Chen, S. Gao, W. Song, *et al.*, "Metasurfaces with planar chiral meta-atoms for spin light manipulation," Nano Lett. **21**(4), 1815–1821 (2021).
12. X. Zeng, D. Rosenmann, D. A. Czaplewski, *et al.*, "Chiral metasurfaces of wavy rectangle resonators with tunable circular dichroism," Optik **286**, 171024 (2023).
13. L. Ouyang, W. Wang, D. Rosenmann, *et al.*, "Near-infrared chiral plasmonic metasurface absorbers," Opt. Express **26**(24), 31484–31489 (2018).
14. M. Khorasaninejad, W. Chen, A. Zhu, *et al.*, "Multispectral chiral imaging with a metalens," Nano Lett. **16**(7), 4595–4600 (2016).
15. F. Walter, G. Li, C. Meier, *et al.*, "Ultrathin nonlinear metasurface for optical image encoding," Nano Lett. **17**(5), 3171–3175 (2017).
16. Y. Chen, J. Gao, and X. Yang, "Chiral grayscale imaging with plasmonic metasurfaces of stepped nanoapertures," Adv. Opt. Mater. **7**(6), 1801467 (2019).
17. W. Li, Z. J. Coppens, L. V. Besteiro, *et al.*, "Circularly polarized light detection with hot electrons in chiral plasmonic metamaterials," Nat. Commun. **6**(1), 8379 (2015).
18. K. J. Miller, R. F. Haglund, and S. M. Weiss, "Optical phase change materials in integrated silicon photonic devices," Opt. Mater. Express **8**(8), 2415–2429 (2018).
19. M. Wuttig, H. Bhaskaran, and T. Taubner, "Phase-change materials for non-volatile photonic applications," Nat. Photonics **11**(8), 465–476 (2017).
20. Y. Zhang, J. B. Chou, J. Li, *et al.*, "Broadband transparent optical phase change materials for high-performance nonvolatile photonics," Nat. Commun. **10**(1), 4279 (2019).
21. A. K. U. Michel, M. Wuttig, and T. Taubner, "Design parameters for phase-change materials for nanostructure resonance tuning," Adv. Opt. Mater. **5**(18), 1700261 (2017).
22. C.-Y. Hwang, G. H. Kim, J.-H. Yang, *et al.*, "Rewritable full-color computer-generated holograms based on color-selective diffractive optical components including phase-change materials," Nanoscale **10**(46), 21648–21655 (2018).
23. M. N. Julian, C. Williams, S. Borg, *et al.*, "Reversible optical tuning of GeSbTe phase-change metasurface spectral filters for mid-wave infrared imaging," Optica **7**(7), 746–754 (2020).
24. S. K. Patel, J. Parmar, V. Sorathiya, *et al.*, "Tunable infrared metamaterial-based biosensor for detection of hemoglobin and urine using phase change material," Sci. Rep. **11**(1), 7101 (2021).
25. Y. Qu, Q. Li, L. Cai, *et al.*, "Thermal camouflage based on the phase-changing material GST," Light: Sci. Appl. **7**(1), 26 (2018).
26. A. Tittl, A. K. U. Michel, M. Schäferling, *et al.*, "A switchable mid-infrared plasmonic perfect absorber with multispectral thermal imaging capability," Adv. Mater. **27**(31), 4597–4603 (2015).
27. B. Tang, Z. Y. Li, E. Palacios, *et al.*, "Chiral-selective plasmonic metasurface absorbers operating at visible frequencies," IEEE Photonics Technol. Lett. **29**(3), 295–298 (2017).
28. X. Zeng, D. Rosenmann, D. A. Czaplewski, *et al.*, "Mid-infrared chiral metasurface absorbers with split-ellipse structures," Opt. Commun. **525**, 128854 (2022).

Optics EXPRESS

29. A. D. Rakić, A. B. Djurišić, J. M. Elazar, *et al.*, "Optical properties of metallic films for vertical-cavity optoelectronic devices," Appl. Opt. **37**(22), 5271–5283 (1998).
30. K. Shportko, S. Kremers, M. Woda, *et al.*, "Resonant bonding in crystalline phase-change materials," Nat. Mater. **7**(8), 653–658 (2008).
31. Y. Chen, T.-S. Kao, B. Ng, *et al.*, "Hybrid phase-change plasmonic crystals for active tuning of lattice resonances," Opt. Express **21**(11), 13691–13698 (2013).
32. A. V. Kiselev, V. V. Ionin, A. A. Burtsev, *et al.*, "Dynamics of reversible optical properties switching of $Ge_2Sb_2Te_5$ thin films at laser-induced phase transitions," Opt. Laser Technol. **147**, 107701 (2022).
33. Q. He, Z. Liu, Y. Lu, *et al.*, "Low-loss ultrafast and nonvolatile all-optical switch enabled by all-dielectric phase change materials," iScience **25**(6), 104375 (2022).